Journal of Mechanical Engineering Research and Developments
ISSN: 1024-1752
CODEN: JERDFO
Vol. 44, No. 5, pp. 10-17
Published Year 2021

Modelling and Simulation of Pitting Corrosion

Bahaa R. Al-Shemmary, Falah Kaify Matloub, Hassan Al-Fetlawi

Department of Chemical Engineering, University of Babylon, Hilla, Babil, Iraq.

*Corresponding Author Email: bahaarhman100@gmail.com; falahkaify@uobabylon.edu.iq

ABSTRACT

Pitting corrosion is one of the most dangerous corrosion types that cause accelerated metal dissolution due to a breakdown of passive protective film on the metal surface. A mathematical simulation of pitting carbon steel corrosion in 1M sodium chloride solution was studied in this work. The commercial software (COMSOL Multiphysics 3.5a) was used to solve the equations that govern this problem. A two-dimensional model that allows the prediction of pit growth of the propagation stage was developed. The simulation model's extracted results show how different parameters such as initial concentration of species, initial pH, different chemical and electrochemical reactions, and range of potential affect the current density and compare the result with the Pourbaix diagram of iron.

KEYWORDS

COMSOL, pitting corrosion, Mathematical model

INTRODUCTION

Pitting corrosion is a form of localized corrosion, where the rate of corrosion in certain areas is higher than in others [1-8]. Pitting corrosion can be seen in certain alloys with a passive film on their surface that protects them from general corrosion. Pitting degradation occurs in some of the most widely used alloys, such as stainless steel and aluminium alloys. Corrosion pits of various shapes and sizes, some of which are "hidden" by a perforated cover, may grow wide and cause catastrophic failure in infrastructure systems subjected to mechanical loadings, such as turbine blades bridges, pipelines, and nuclear power plants [9-11]. Corrosion pits regulated by chemical reactions and determined by environmental and mechanical loading conditions across length scales may result in embrittlement (loss of ductility) and major strength decreases [12]. Computational simulations can now implement mathematical models to replicate complicated multi-physics processes with high resolution, thanks to technological advancements in recent decades and a significant rise in computing capacity. Once optimized and accepted against carefully performed studies, computer models will broaden the scope of laboratory investigations to more practical settings and duration and time scales that would be impossible to examine otherwise. These models are mathematical, and they can predict pit depth over time based on those input parameters [13]. Knowing that defeat does not often start from the pitting bottom, more thorough experiments are warranted for learning the capacity to predict failures and then design against them [14]. Models use various computational approaches to solve the pitting mechanism's advancement in more detail: the development of pits' form and composition, the amount of various chemical species within and outside of the trap, the distribution of electrical potential across the domain of interest, etc. Reactions kinetics at the degradation front and the pits' chemical species' transportation kinetics are generally taken as the basis for these models.

COVERING EQUATION

The Nernst-Planck Equation(N-P), as defined in eq (1), is often utilized to explain ion transfer since convection, migration, and diffusion in the ion transport phase. Each ion's movement because of the device's potential electric fields is believed to be independent of the diffusion term [15].

$$\frac{\partial[\mathrm{i}]}{\partial \mathrm{t}} = \mathrm{D_i}\Phi^2[\mathrm{i}] + \mathrm{Z_i}\,\mathrm{U_i}\mathrm{F}\nabla([\mathrm{i}]\nabla\Phi) + \mathrm{R_i} \quad (1)$$

Where [i] is the concentration of species i, D is the effective diffusion coefficient, Z is the charge number, U_i is the mobility (given that $U_i=\frac{D_i}{RT}$), R is the production rate/depletion of i, and $\nabla\Phi$ is the potential gradient. The Butler–Volmer formula, which gives an average free-energy implementation of charge transfer, but does not analyze the particular processes involved in the transfer, is included in most electrical and chemical kinetic models. The Butler-Volmer equation, which represents the current density at an electrode in terms of the overpotential, describes an electrochemical reaction rate [16]. The form of Butler–Volmer formula as specified in eq (2) below:

$$i = i_0 \left(\exp\left[a_1 F\frac{(V_m-\Phi)}{RT}\right]\exp\left[-a_2 F\frac{(V_m-\Phi)}{RT}\right]\right) \quad (2)$$

Where: i denote electrode current density (A/m^2), i_0 is the current exchange density (A/m^2), V_m is the electrode potential(V), Φ is the equilibrium potential(V), T is the absolute temperature(K), F is the Faraday constant, R is the universal gas constant, a1=anodic charge transfer coefficient, a2=cathodic charge transfer coefficient. In this model, the Tafel expressions are given by Turnbull for iron dissolution and hydronium reduction, i.e. [14]:

Current density for iron oxidation, $i_1 = i_{01}\exp\left[a_1 F\frac{(V_m-\Phi)}{RT}\right]$ (3)

Current density required for proton decrement, $i_2 = i_{02}[H]\exp\left[a_2 F\frac{(V_m-\Phi)}{RT}\right]$ (4)

Where i_{01}, i_{02} exchange current density (A/m^2) for iron dissolution and hydrogen reduction respectively, i_1, i_2 electrode current density (A/m^2) for iron dissolution and hydrogen reduction respectively,

MODEL ASSUMPTIONS

In order to simulate the corrosion phenomenon of a single pit, specific assumptions are established initially, which are mentioned below:

(i) Transport equations for dilute solution theory are considered and ignoring the interactions between dissolved chemical.
(ii) Effects from the transport of aqueous chemical species due to convection are neglected.
(iii) Effects of a double layer are not considered, and local electroneutrality within the pit electrolyte is assumed.
(IV) Alloying ingredient are not considered (e.g., nickel or chromium). Only iron is considered as it is the greatest constituent in carbon steel.
(V) mass transport in through-thickness was neglected.

REACTIONS

The reactions taking place are classified depending on the place where they occur. So, the reactions that take place at the electrode are represented as electrochemical reactions, while the reactions that occur at the solution are represented as homogeneous reactions [15].

Electrochemical reactions

The corrosion model of a pit is composed of three electrochemical reactions; the metal dissolution (anodic) process for the active wall is given by:

$$Fe \longrightarrow Fe^{+2} + 2e^- \quad (5)$$

The reactions that occur at the cathode are described by oxygen reduction in eq (6) and hydrogen reduction in eq (7).

$$O_2 + 2H2O + e^- \longrightarrow 4OH \quad (6)$$

$$H^+ + e^- \longrightarrow H_2 \quad (7)$$

Homogeneous reactions

The homogeneous reactions in the solution are iron hydrolysis in Equation (8), water dissociation in Equation (9), with an addition of two more reactions are a product of the $FeCl^+$ complex in equation (10), and hydrogen gas formation H2 by an electrochemical decrement in Equation (7).

$$Fe^{+2} + H_2O \longrightarrow FeOH^+ + H^+ \quad (8)$$

$$H_2O \longrightarrow H^+ + OH^+ \quad (9)$$

$$Fe^{+2} + Cl^- \longrightarrow FeCl^+ \quad (10)$$

Because of the bulk chlorine solution, the FeCl+ complex was used in the model. It is added for hydrogen gas production because hydrogen is a result of cathodic reactions and can be formed even though the possibility is anodic [17]. Sodium ions in sodium chloride solution are not included in the chemical reaction but are included to keep the electroneutrality across the mouth of pitting:

$$NaCl_{(aq)} \longrightarrow Na^+ + Cl^- \quad (11)$$

Depending to Sharland, six aqueous chemical species have been essential to creating a basic iron corrosion model; moreover, two other species added by [18,19]: Fe^{+2}, H^+, OH^-, Cl^-, Na^+, $FeOH^+$, $FeCl^+$ and H_2

BOUNDARY CONDITION

This paradigm is only investigated within the pit, and it is ignored outside of it. The fluxes of the ions included in the electrochemical oxidation at the pit's tip and bulk amount at the mouth are the boundary cases assumed in the pit model. At the passive wall, no reduction or dissolution occurs that is mean no production or depletion of ion occur as below:

At the mouth of pit $C_i=C_{i0}$ $\nabla\Phi = 0$ (12)

At passive wall $D_{Ci} - [\nabla^2 C_{Ci} \frac{F}{RT}\nabla(C_{Ci}\nabla\Phi)]=0$ (13)

At active wall $D_{Ci} - [\nabla^2 C_{Ci} \frac{F}{RT}\nabla(C_{Ci}\nabla\Phi)]= \frac{i_1}{ZF}$ (14)

$$D_{Ci} - [\nabla^2 C_{Ci} \frac{F}{RT}\nabla(C_{Ci}\nabla\Phi)]= \frac{i_2}{ZF} \quad (15)$$

Whereas; C_i is the species' amount, C_{i0} is the bulk amount.

NUMERICAL METHOD

The governing equations were solved numerically using COMSOL Multiphysics 3.5a depending on the finite-element technique. COMSOL Multiphysics is an effective interactive kit designed for modelling and solving all kinds of problems in science and engineering. The pit is presented in rectangular geometry with a curved bottom (set as electrochemically active). In the figure below illustrate the mesh of geometry that contain 325 mesh point and 582 elements.

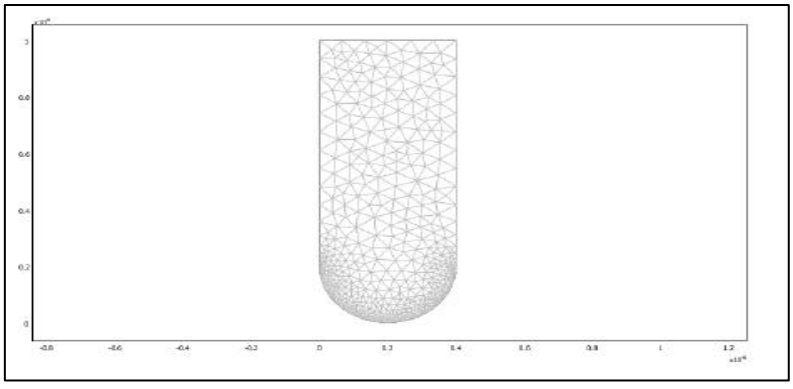

Figure 1. Mesh geometry of the pit

RESULT AND DISCUSSION

In this section, a part of what was obtained from the modelling program is shown with a simple explanation of the presented figures. From Figure 2 below, the ferrous ion (Fe^{+2}) concentration observes a gradual rise with increasing applied potentials due to an increasing electrochemical rate of the metal dissolution process. At the mouth, which acts as bulk concentration, Fe^{+2} remains constant while increasing inside and bottom of the pit since the pit's bottom is electrochemically active where the dissolution of iron occurs.

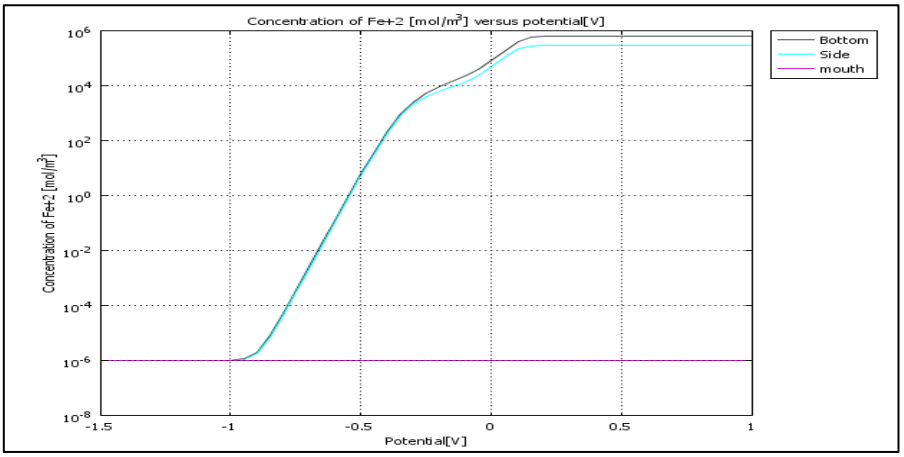

Figure 2. Amount of Fe^2 at three-point along with the pit.

The increase in iron dissolution from the bottom will make the region rich in positive charges, which causes the negative ions (chlorine ion) to migrate from the bulk to attract positive charges, as shown in figure (3) concentration increases in bottom and side as potential increase. Figure 4 shows the electrolyte pH at the electroactive surface (bottom of the pit) as a function of metal potentials, where the electrolyte experiences a rise in the pH with increasing cathodic potential. At lower anodic potentials, a steep drop in pH is observed, which can be referred to as an increased metal hydrolysis rate. Despite the sudden drop, the pH profile observes a slope change (from -0.6 V onwards) at higher anodic potentials. The potential electrolyte influences the metal dissolution process resulting in fewer Fe^{+2} ions ready to undergo hydrolysis. This, subsequently, cause fewer productions of protons, causing the pH to observe smaller changes.

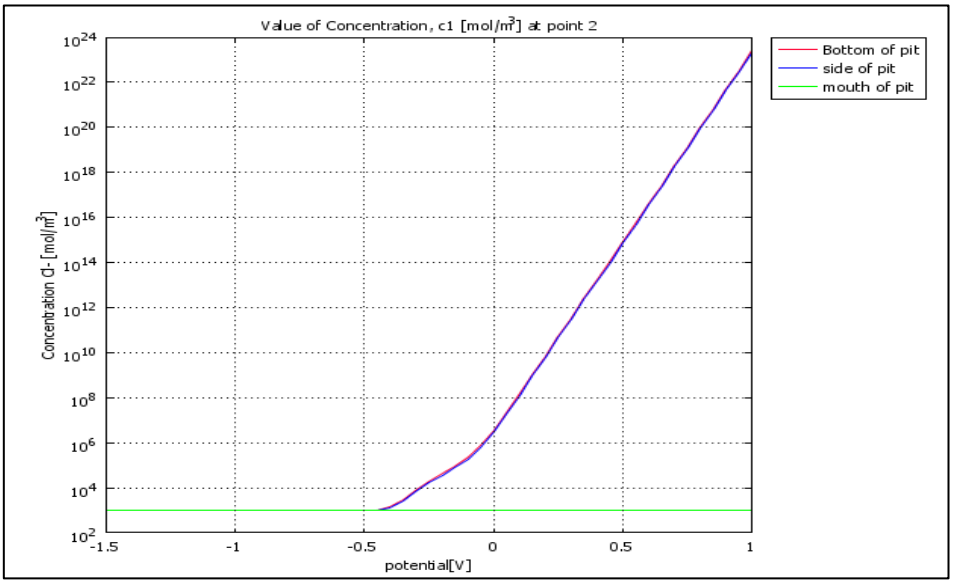

Figure 3. Amount of Cl^- at three-point along with pit

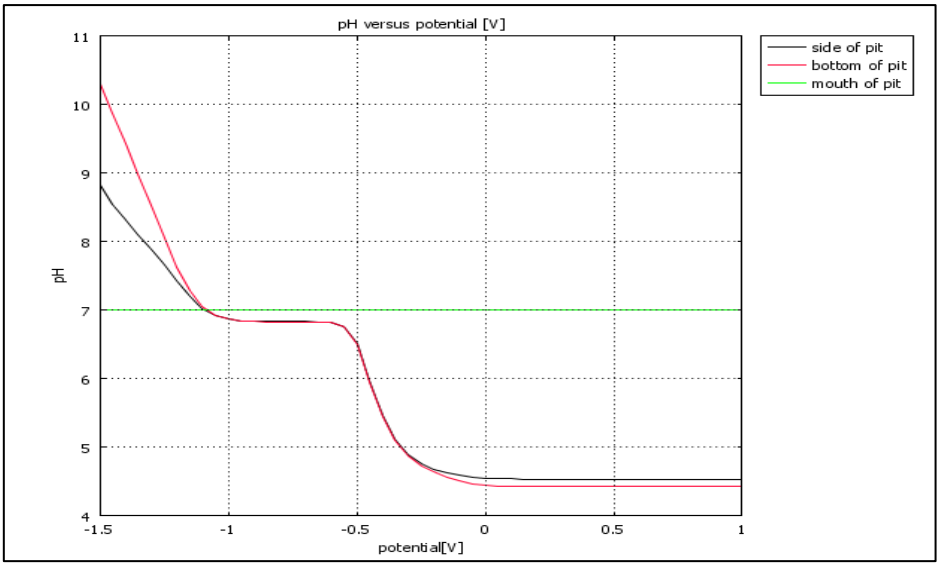

Figure 4. Electrolyte pH profile as a function of metal potentials at three-point along pitting.

It is possible to see the hydrogen bubbles as iron alloys are immersed in an acidic solution and are inactive. Metal ion Fe+2 is formed immediately, and hydrogen ions are decreased at the same time. This is a simple operation, and hydrogen gas should be noticeable at this stage. This is shown by the model in Figure 5, which depicts a rapid 'jump' in the 'amount' of hydrogen gas due to hydrogen to proton reductions.

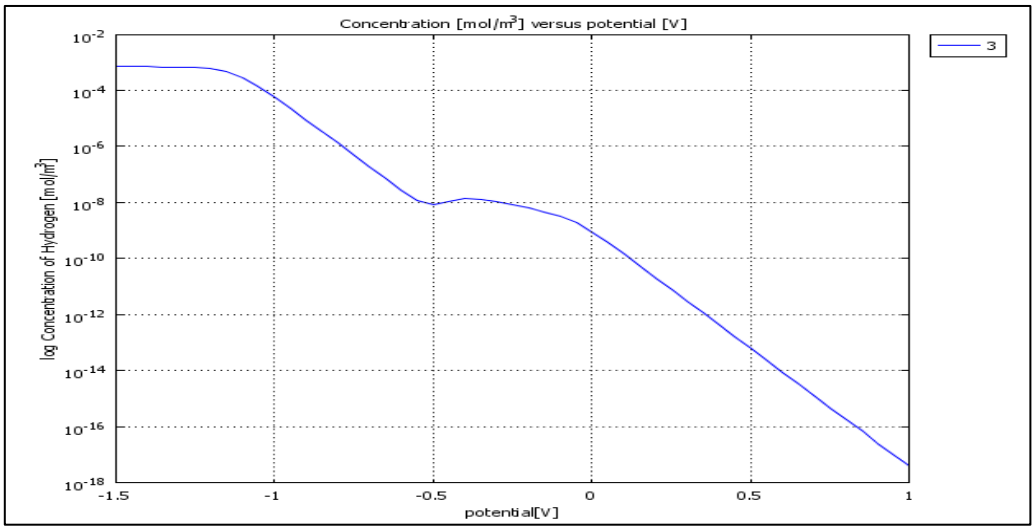

Figure 5. Amount of Hydrogen as a potential role at the bottom of pitting.

Figure 6 indicates that at the bottom of the trap, metal ions Fe+2 continue to accumulate slowly. The model is set to be electrochemically active in this field. The increasing amount of Fe+2 at the pit's bottom indicates that metal dissolution is continuing. Fe+2 continues to accumulate at the greater part of the hole, which could also be seen in the figure. This is consistent with diffusion, which states that animals migrate from high to low concentrations. In this scenario, the amount of Fe+2 has reached a point where the ions of metal diffuse to the passive area further up the pit, where the amount of Fe+2 is smaller. As described by, Fe+2 is supposed to hit a stage where it can disperse out of the trap, encouraging metal dissolution and forming general corrosion on the metal surface [20]. The effect of the potential is also shown in the figure below) fig.6), in which the dissolution density rises as the potential grows more optimistic.

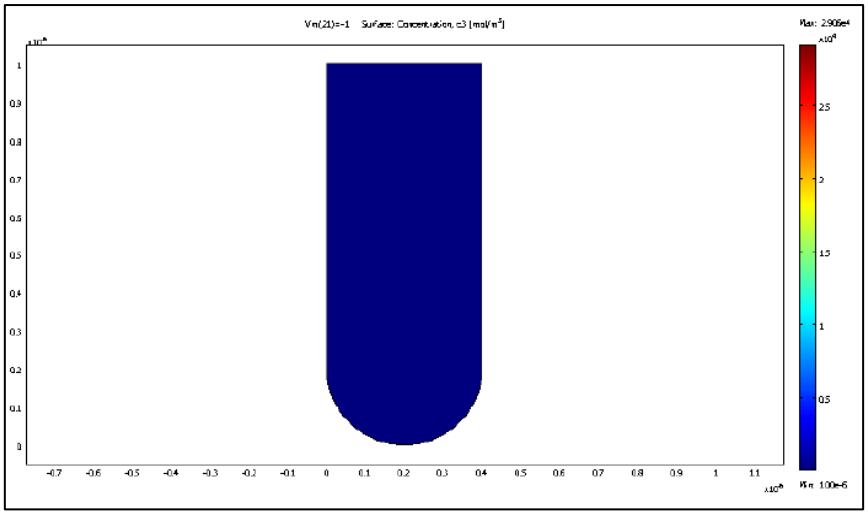

(i) Amount of Fe^{+2} potential at -1 volt

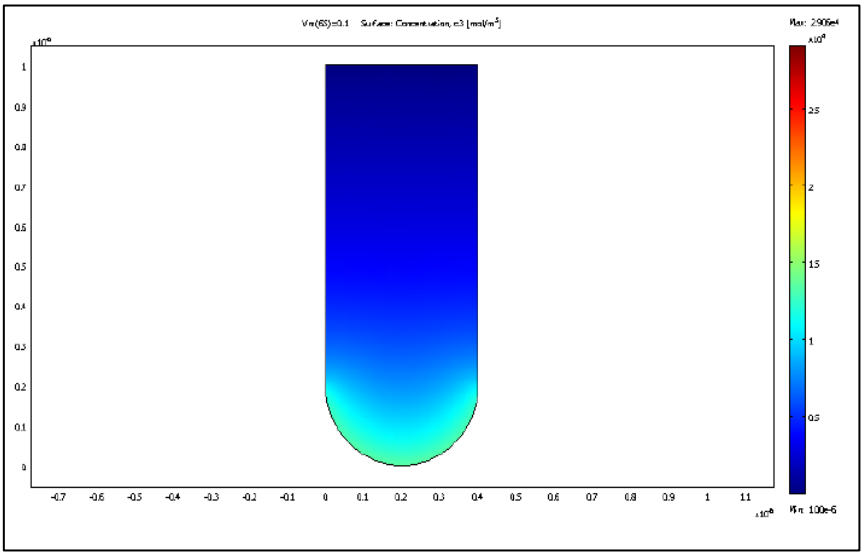

(ii) Amount of Fe^{+2} potential at 0.1 volt

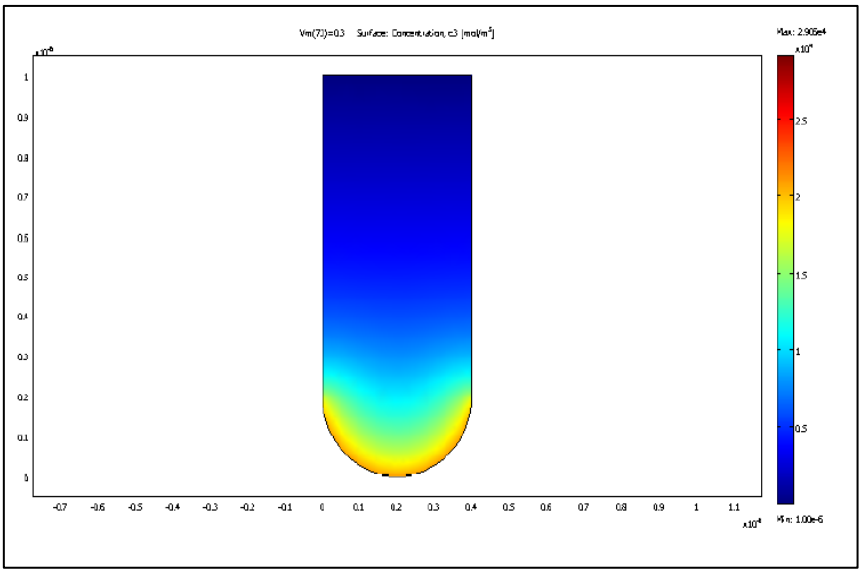

(iii) Amount of Fe^{+2} at potential 0.3 volt

Figure 6. Figures (i)-(iii) show that Fe^{+2} accumulation happens at the pit's bottom concerning potential. From Figure 5, it is found that hydrogen gas decreases almost suddenly, starting from -0.3. If this value is compared with the paurbax diagram in figure7 , it is found to be intersecting at point A where water is thermodynamically stable instead of hydrogen, while the hydrogen is stable under this point. Hydrolysis is one of the most important reactions considered in the model, where water reacts with Fe+2 to create H+ and FeOH+. This means that the reaction continues with the continuation of iron dissolution, as shown in Figure 8 that this reaction begins to occur at approximately -0.65[V]. If this value is compared with the paurbax diagram in figure 7, it is found to be intersecting at point B, which is located between immunity and corrosion zone, and this shows that Fe+2 ion is produced at such condition (pH and potential).

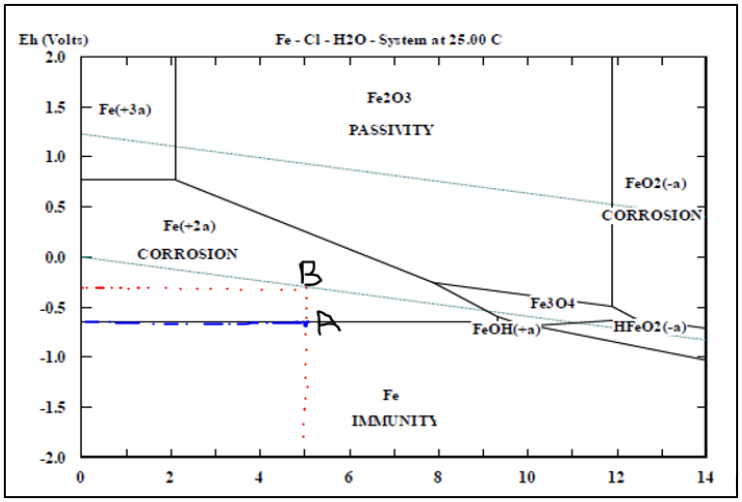

Figure 7. Pourbaix schematic diagram point A, in which the model shows a metal ion predominance, Fe+2. Furthermore, B, in which the model depicts the depletion of hydrogen gas, H2 [21]s.

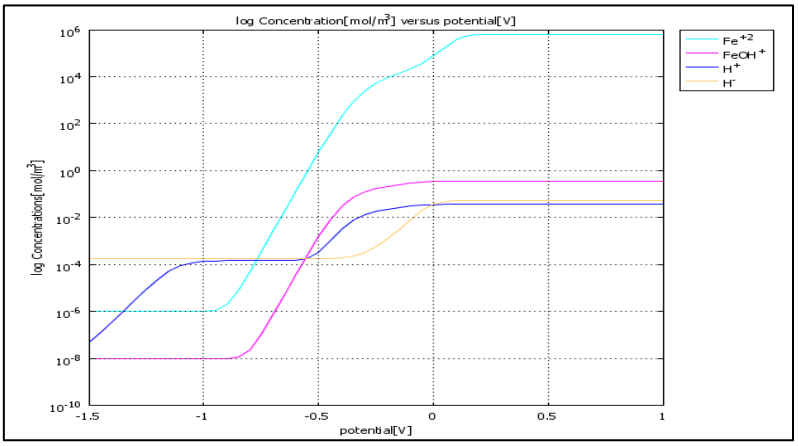

Figure 8. Concentration of spices as a function of potential

CONCLUSION

The model's regulating formula in this study is based on anodic dissolution and transportation kinetics in the electrolyte. The model shows the importance of each parameter that was introduced in the model, how iron dissolution is affected by other equilibrium reactions, the effect of each on the other, the acidity of the medium and the initial concentrations of each species, the extent to which the potential range is affected., and finally to what a degree the results are consistent with what has been investigated in the literature.

REFERENCES

[1] D. A. Jones, "Principles and prevention of corrosion", Macmillan, 1992.

[2] G.S. Frankel, "Pitting corrosion of metals: a review of the critical factors", J. Electrochem. Soc., Vol. 145, No. 6, Pp., 2186, 1998.

[3] R.W. Revie, "Corrosion and corrosion control: an introduction to corrosion science and engineering", John Wiley & Sons, 2008.

[4] S. Jafarzadeh, Z. Chen, and F. Bobaru, "Computational modeling of pitting corrosion", Corros Rev, Vol. 37, No. 5, Pp. 419–439, 2019. doi: 10.1515/corrrev-2019-0049.

[5] N.M. Dawood, N.S. Radhi, and Z.S. Al-khafaji, "Investigation Corrosion and Wear Behavior of Nickel-Nano Silicon Carbide on Stainless Steel 316L", Vol. 1002, Pp. 33–43, 2020.

[6] N.S. Radhi and Z. Al-Khafaji, "Investigation biomedical corrosion of implant alloys in physiological environment", Int. J. Mech. Prod. Eng. Res. Dev., Vol. 8, No. 4, 2018.

[7] N.S. Radhi, M. Marza, and Z.S. Al-Khafaji, "Modification of Nickel-phosphor Electroless Coatings by adding particles of Zirconia", Solid State Technol., Vol. 63, No. 2, 2020.

[8] M. Jabor, N.S. Radh, M.A. Al-kinani, and Z.S. Al-khafaji, "Optimization of Electro less of Nickel base coating for Cermet Cutting Tools Substrate", Vol. 44, No. 3, Pp. 30–40, 2021.

[9] S. Rani, A.K. Agrawal, and V. Rastogi, "Failure analysis of a first stage IN738 gas turbine blade tip cracking in a thermal power plant", Case Stud Eng Fail Anal., Vol. 8, Pp. 1–10, 2017.

[10] N.S. Radhi and Z.S. Al-Khafaji, "Preparation and Investigation composite coating (Ni-nano hydroxyapatite) on low carbon steel samples".

[11] Y. Zhu, X. Qian, Z. Liu, P. Huang, and M. Yuan, "Analysis and assessment of the Qingdao crude oil vapor explosion accident: Lessons learnt", J. Loss Prev Process Ind., Vol. 33, Pp. 289–303, 2015.

[12] S. Li, Z. Chen, L. Tan, and F. Bobaru, "Corrosion-induced embrittlement in ZK60A Mg alloy", Mater. Sci. Eng. A., Vol. 713, Pp. 7–17, 2018.

[13] A. Valor, F. Caleyo, L. Alfonso, D. Rivas, and J.M. Hallen, "Stochastic modeling of pitting corrosion: a new model for initiation and growth of multiple corrosion pits", Corros Sci., Vol. 49, No. 2, Pp. 559–579, 2007.

[14] A. Turnbull, L. Wright, and L. Crocker, "New insight into the pit-to-crack transition from finite element analysis of the stress and strain distribution around a corrosion pit", Corros Sci., Vol. 52, No. 4, Pp. 1492–1498, 2010.

[15] J.L.D. La Cruz, "Numerical strategies for corrosion management: spatial statistics and finite element simulation", 2008.

[16] M. Raunio, "Basic approaches and goals for crevice corrosion modelling", Pp. 50, 2015, [Online]. Available: http://www.vtt.fi/inf/julkaisut/muut/2015/VTT-R-02078-15.p

[17] B. Vuillemin, R. Oltra, and R.A. Cottis, "Use of a general-purpose finite element package for modeling of crevice corrosion", Corros NACE Int House, 2004.

[18] S.M. Sharland, C.P. Jackson, and A.J. Diver, "A finite-element model of the propagation of corrosion crevices and pits", Corros Sci., Vol. 29, No. 9, Pp. 1149–1166, 1989.

[19] S. Salleh, "Modelling pitting corrosion in carbon steel materials", The University of Manchester (United Kingdom), 2013.

[20] R.D. Grimm and D. Landolt, "Salt films formed during mass transport-controlled dissolution of iron-chromium alloys in concentrated chloride media", Corros Sci, Vol. 36, No. 11, Pp. 1847–1868, 1994.

[21] A.A. Shubbar, Z.S. Al-khafaji, M.S. Nasr, and M.W. Falah, 'Using Non-Destructive Tests for Evaluating Flyover Footbridge: Case Study'.